

Loss in solid-core photonic crystal fibers due to interface roughness scattering

P. J. Roberts^{1,2}, F. Couny^{1,2}, H. Sabert², B. J. Mangan², T. A. Birks¹, J. C. Knight¹ and P. St. J. Russell¹

¹ Department of Physics, University of Bath, Claverton Down, Bath BA2 7AY, United Kingdom.

² BlazePhotonics Ltd, University of Bath Campus, Claverton Down, Bath BA2 7AY, United Kingdom

pir20@bath.ac.uk

Abstract: The loss resulting from roughness scattering at hole interfaces within solid core photonic crystal fibers is theoretically analyzed and compared with measurements on fabricated fibers. It is found that a model roughness spectrum corresponding to frozen in capillary waves gives results in reasonably good agreement with experiments on small core fibers. In particular, the roughness scattering loss is shown to be only weakly dependent on wavelength. Agreement at a larger core size requires a long length-scale cut-off to be introduced to the roughness spectrum. Due to the long range nature of the roughness correlations, the scattering is non Rayleigh in character and cannot be interpreted in terms of a local photon density of states.

©2005 Optical Society of America

OCIS codes: (060.2310) Fiber optics; (060.2400) Fiber properties; (290.5880) Scattering, rough surfaces

References and links

1. J. Schroeder, "Light scattering in glass," in *Treatise on Materials Science and Technology Vol. 12*, M. Tomozawa and R. H. Doremus, eds. (Academic Press, 1977)
2. P. J. Roberts, F. Couny, H. Sabert, B. J. Mangan, D. P. Williams, L. Farr, M. W. Mason, A. Tomlinson, T. A. Birks, J. C. Knight and P. St. J. Russell, "Ultimate low loss of hollow-core photonic crystal fibers," *Opt. Express* **13**, 236-244 (2005)
<http://www.opticsexpress.org/abstract.cfm?URI=OPEX-13-1-236>
3. B. J. Mangan, L. Farr, A. Langford, P. J. Roberts, D. P. Williams, F. Couny, M. Lawman, M. Mason, S. Coupland, R. Flea, H. Sabert, T. A. Birks, J. C. Knight and P. St. J. Russell, "Low loss (1.7 dB/km) hollow core photonic band gap fibre," in *Proc. Optical Fiber Commun. Conf.* (Los Angeles, 2004), post-deadline paper PDP24
4. P. J. Roberts, F. Couny, T. A. Birks, J. C. Knight, P. St. J. Russell, B. J. Mangan, H. Sabert, D. P. Williams and L. Farr, "Achieving low loss and low nonlinearity in hollow core photonic crystal fibers," in *Proc. CLEO 2005* (Baltimore, 2005), paper CWA7
5. J. A. West, C. M. Smith, N. F. Borrelli, D. C. Allan, and K. W. Koch, "Surface modes in air-core photonic band-gap fibers," *Opt. Express* **12**, 1485-1496 (2004)
<http://www.opticsexpress.org/abstract.cfm?URI=OPEX-12-8-1485>
6. T. Hasegawa, E. Sasaoka, M. Onishi, M. Nishimura, Y. Tsuji, and M. Koshihara, "Hole-assisted lightguide fiber for large anomalous dispersion and low optical loss," *Opt. Express* **9**, 681-686 (2001)
<http://www.opticsexpress.org/abstract.cfm?URI=OPEX-9-13-681>
7. L. Farr, J. C. Knight, B. J. Mangan and P. J. Roberts, "Low loss photonic crystal fiber," in *European Conference on Optical Communication* (Copenhagen, 2002), post-deadline paper PD13
8. F. Couny, H. Sabert, P. J. Roberts, D. P. Williams, A. Tomlinson, B. J. Mangan, L. Farr, J. C. Knight, T. A. Birks and P. St. J. Russell, "Visualization of the photonic band gap in hollow core photonic crystal fibers using side scattering," *Opt. Express* **13**, 558-563 (2005)
<http://www.opticsexpress.org/abstract.cfm?URI=OPEX-13-2-558>
9. L. D. Landau and E. M. Lifshitz, *Theory of Elasticity* (Oxford: Pergamon, 1970)
10. J. Jäckle and K. Kawasaki, "Intrinsic roughness of glass surfaces," *J. Phys.: Condens. Matter* **7**, 4351-4358 (1995)
11. J. Meunier, "Liquids interfaces: role of the fluctuations and analysis of ellipsometry and reflectivity measurements," *J. Phys. France* **48**, 1819-1831 (1987)

12. A. W. Snyder and J. D. Love, *Optical Waveguide Theory* (Chapman and Hall, London, 1983)
13. M. Skorobogatiy, S. A. Jacobs, S. G. Johnson, and Y. Fink, "Geometric variations in high index-contrast waveguides, coupled mode theory in curvilinear coordinates," *Opt. Express* **10**, 1227-1243 (2002) <http://www.opticsexpress.org/abstract.cfm?URI=OPEX-10-21-1227>
14. S. G. Johnson, M. Ibanescu, M. A. Skorobogatiy, O. Weisberg, J. D. Joannopoulos and Y. Fink, "Perturbation theory for Maxwell's equation with shifting material boundaries," *Phys. Rev. E* **65**, 066611 (2002)
15. S. G. Johnson, M. Ibanescu, M. L. Povinelli, M. Soljacic, A. Karalis, S. Jacobs, D. Roundy, Y. Fink and J. D. Joannopoulos, "Anomalous loss and propagation in photonic-crystal waveguides," presented at PECS-VI, Aghia Pelaghia, Crete, June 2005
16. S. Hughes, L. Ramunno, J. F. Young and J. E. Sipe, "Extrinsic optical scattering loss in photonic crystal waveguides: Role of fabrication disorder and photon group velocity," *Phys. Rev. Lett.* **94**, 033903 (2005)
17. F. Seydou, O. Ramahi, R. Duraiswami and T. Seppanen, "Computation of Green's Function for Finite-Size Photonic Crystals by Boundary Element Method," in *IEEE Antennas and Propagation Society Symposium* (Monterey, USA, June 20-25, 2004), Vol. 4, pp. 4320-4323
18. T. P. White, B. T. Kuhlmey, R. C. McPhedran, D. Maystre, G. Renversez, C. M. de Sterke and L. C. Botten, "Multipole method for microstructured optical fibers: I. Formulation," *J. Opt. Soc. Am. B* **19**, 2322-2330 (2002)
19. D. P. Fussell, R. C. McPhedran, C. M. de Sterke, "Three-dimensional Green's tensor, local density of states, and spontaneous emission in finite two-dimensional photonic crystals composed of cylinders," *Phys. Rev. E* **70**, 066608 (2004)
20. R. F. Cregan, J. C. Knight, P. St.J. Russell and P. J. Roberts 1999, "Distribution of spontaneous emission from an Er³⁺-doped photonic crystal fiber," *J. Lightwave Tech.* **17**, 2138-2141 (1999)
21. P. J. Roberts and T. J. Shepherd, "The guidance properties of multi-core photonic crystal fibres," *J. Optics A: Pure and applied* **3**, S133-S140 (2001)
22. J.C. Knight, T.A. Birks, P.St.J. Russell and J.G. Rarity, "Bragg scattering from an obliquely illuminated photonic crystal fiber," *Appl. Opt.* **37**, 449-452 (1998)

1. Introduction

Photonic crystal fibers (PCFs) comprise an array of parallel air holes in a glass matrix which surround a guiding core. The large index step which exists between silica and air opens up avenues for mode control which are not accessible to conventional doped-fiber technology. In many applications, such as long haul communication, fiber loss plays a key role. It is thus important to understand the level to which PCF loss can be reduced by improvement in fabrication processes. In conventional fibers, this limit is well understood, being set by Rayleigh scattering and Infra-red absorption within bulk glass [1]. The former loss mechanism is a result of short range index fluctuations within the bulk material which are of thermodynamic origin and as such is not amenable to significant reduction by technological improvements. The latter loss mechanism, which is due to multi-phonon processes, is an intrinsic property of the glass. The combined influence of these loss mechanisms has been to limit the loss of telecom fiber to around 0.15 dB/km.

The presence of glass / air interfaces in PCFs introduces new mechanisms for the incursion of loss. Impurity ingress occurring at the interfaces during the fiber draw may increase the loss due to absorption, or may act as centers of formation for crystallites which add to the scattering loss. These loss contributions can be reduced or eliminated by technological improvements of fiber fabrication. There remains, however, a scattering contribution to loss which is due to the inherent roughness of the interfaces. Such roughness arises from thermally excited surface capillary waves (SCWs), which become frozen-in during the fiber draw at the glass transition temperature [2]. This roughness forming process is dictated by equilibrium thermodynamics, so that it can not be substantially reduced by technological improvements.

The loss floor in hollow core PCFs has been shown to be dominated by the surface roughness scattering, the loss component due to bulk glass being greatly suppressed since most of the light propagates in air. The philosophy to loss reduction for these fibers entails incorporating antiresonant features into the design which act to decrease the field strength of the core guided mode at the interfaces [2-4], or minimizing as far as possible the occurrence

of surface guided modes within the band gap [5]. The situation for solid core PCFs is less clear, since for these fibers most of the mode field propagates in the glass and is thus subject to its loss characteristics. The loss of solid core PCFs is found to increase as the core size decreases, a property which has been ascribed to the increased field strength at the hole interfaces leading to a larger roughness scattering loss component [6,7]. A goal of the current paper is to provide *ab initio* calculations of surface interface roughness loss suffered in solid core PCFs, based on a model roughness spectrum of SCWs which is introduced in section 2. A summary of the theoretical basis for the calculation, in which the electric field Green tensor plays a central role in conjunction with a function related to the roughness power spectrum, is given in section 3. More details on the scattering formulation are deferred to appendix A. Section 4 compares the calculated angular dependence of the light scattered due to SCW roughness with measurements obtained using the experimental technique described in [8]. The angular dependence serves to emphasize the non Rayleigh nature of the scattering. In section 5, the wavelength dependence of the SCW scattering loss is calculated for an example small-core PCF. The results are compared with the measured loss spectrum of a fabricated fiber with a similar geometry. This section also considers SCW roughness scattering for a solid core PCF with larger core size, which requires the introduction of a long length-scale cut-off to the roughness spectrum to gain correspondence with experiment. Further details on the numerical evaluation of the total roughness scattering loss are given in appendix B. Conclusions are presented in section 6.

2. Roughness at hole interfaces

The surface of a liquid in thermal equilibrium is not flat due to the thermal excitation of surface capillary waves (SCWs). Such fluctuations exist on the surface of molten glass and become frozen-in as it is taken through the glass transition temperature T_g during the fiber drawing process. Despite the increase in the material stiffness associated with glass formation, the dynamics and energy balance associated with the glass transition unfortunately does not lead to a reduction in amplitude of the SCWs from their thermal equilibrium values in the liquid state just above T_g : the surface that results after the transition has occurred can be considered simply as a snapshot of the surface that exists on a molten surface just above the glass transition temperature.

Since the thermal distribution of energy between the SCW modes is an entirely incoherent process, the sum of the contributions from all the SCWs yields a rough surface which must be described statistically. For an infinitely extended 2-D interface, the energy per unit area of a SCW with 2-D wavevector \mathbf{k}_{SCW} and amplitude A is given by

$$E = \frac{1}{4} |A|^2 \sigma |\mathbf{k}_{\text{SCW}}|^2, \quad (1)$$

which is due entirely to work done against the surface tension force [9]. The surface tension has been denoted by σ . Ascribing an average energy of $k_B T_g / 2$ to each surface capillary wave component leads to a roughness power spectrum

$$\tilde{\Psi}(\mathbf{k}_{\text{SCW}}) = \frac{k_B T_g}{\sigma} \frac{1}{|\mathbf{k}_{\text{SCW}}|^2} \quad (2)$$

for the extended interface [10]. The roughness spectrum given in Eq. (2) is scale-free, *i.e.* it describes a statistical fractal interface.

The spectrum describing the rough interfaces within a PCF become quantized due to the closed nature of a hole perimeter. Ignoring any interaction between SCWs on neighboring holes and any effects related to the curvature of the (statistically averaged) hole interface, the roughness spectrum at a hole with perimeter length S can be approximated by

$$\tilde{\Psi}_m(\beta) = \frac{k_B T_g}{\sigma} \frac{1}{S} \frac{1}{[k_s^{(m)2} + \beta^2]}, \quad (3)$$

where $k_s^{(m)} = 2\pi m/S$ is the tangential wavevector component, the index m takes all integer values and β is the wavevector component along the hole axis direction. The spectrum has been normalized such that the roughness height correlation function is determined from

$$\langle h(s, z)h(s + \Delta s, z + \Delta z) \rangle = \frac{1}{2\pi} \sum_{m=-\infty}^{\infty} \exp(im\Delta s) \int_{-\infty}^{\infty} d\beta \exp(i\beta\Delta z) \tilde{\Psi}_m(\beta), \quad (4)$$

where s is the spatial coordinate which defines position around the hole perimeter and z is the coordinate along the axial direction.

Atomic force microscope (AFM) measurements of the roughness spectrum on the interfaces within silica PCF show that it is consistent with Eq. (3) over the scale-range covered by the measurements (approximately 80 nm to 8 μ m) when the surface tension is taken to be around 1 Jm⁻² [2]. The roughness measurement was just taken along the axial direction of the hole, so only correspondence of $\sum_{m=-\infty}^{\infty} \tilde{\Psi}_m(\beta)$ could be checked. The value $\sigma=1.0$ Jm⁻² is somewhat higher than the value $\sigma=0.3$ Jm⁻² measured at an interface prepared in standard atmosphere. It has been postulated the discrepancy can be attributed to the water reduction steps that are maintained during the fiber fabrication process.

The magnitude of the roughness over a decade of length scales which are short compared to the hole perimeter length can be estimated using Eq. (2) to be 0.06 nm, assuming the value $\sigma=1.0$ Jm⁻² and taking $T_g \sim 1500$ K. The characteristic magnitude of the SCW roughness is far smaller than the interface roughness currently achievable by etching techniques, which is perhaps the main reason why the loss achieved in band gap fiber waveguides is orders of magnitude lower than that which has been demonstrated in other band gap waveguide forms.

The roughness spectrum in Eq. (3) leads to a divergence of the integral determining the correlation function in Eq. (4). In practice, the inverse power-law form of the spectrum will eventually become cut-off at both long and short length scales, which serves to render the correlation function expressed in Eq. (4) convergent. At the short length scale end, the cut-off may ultimately be due to the atomic nature of the material leading to a breakdown of the continuum theory which forms the basis of Eq. (3), or may be due to inter-SCW mode-coupling [11]. The long scale cut-off of the spectrum describing fluctuations on an isolated infinitely extended 2-D interface is provided by an external potential such as gravity [10], but for holes in a PCF, the interactions between the interfaces may provide a substantially shorter cut-off scale. The presence of such a reduced long scale cut-off is inferred in section 5 from the roughness scattering loss of large core PCF.

3. Theory of interface roughness scattering loss in photonic crystal fibers

Since the roughness at the interfaces is of small amplitude, the scattering it induces can be calculated by application of perturbation theory. Care must be taken in formulating perturbation methods in electromagnetism when the refractive index steps are sizeable and the perturbations cause the boundaries to shift [12-15], as is the case at PCF interfaces. This is linked to the discontinuity in the component of the **E**-field which is normal to the interfaces. In general, local field corrections need to be incorporated which depend on the polarisation properties of the roughness features at the interface [15]. It will be assumed that short length scale cut off to the roughness spectrum is such that the direction of the local normal to the interface does not fluctuate strongly due to the roughness, so that a difficult local field calculation associated with the continuously rough interface can be avoided. For such roughness, local mode coupling theory can be used to calculate the scattering loss [12]. This approach is preferred over standard (non-local) mode coupling theory or a direct application of the Born series since the field discontinuity is properly handled. Details of the roughness

scattering calculation are presented in Appendix A. The roughness scattering loss is found to be given by

$$\gamma_1 = -\frac{k^3}{4\pi} \left(\frac{\epsilon_0}{\mu_0} \right)^{1/2} (n_g^2 - 1)^2 \text{Im} \left[\sum_{j=1}^{N_{\text{holes}}} \oint_{\text{perimeter}}^{j\text{th hole}} d s \oint_{\text{perimeter}}^{j\text{th hole}} d s' \int d \beta \hat{\mathbf{e}}_1^H(\mathbf{r}_j^-(s')) \mathbf{G}_{2D}(\mathbf{r}_j^+(s'), \mathbf{r}_j^+(s); k, \beta) \hat{\mathbf{e}}_1(\mathbf{r}_j^-(s)) \tilde{\Psi}_j(s, s'; \beta_1 - \beta) \right], \quad (5)$$

where n_g is the refractive index of the glass, $k = 2\pi/\lambda$ is the free-space wavenumber of the light, $\hat{\mathbf{e}}_1(\mathbf{r}_j^-(s))$ and β_1 express the electric field of the guided mode just inside the perimeter of the j 'th hole and the propagation constant of this mode, respectively. $\mathbf{G}_{2D}(\mathbf{r}_j^+(s'), \mathbf{r}_j^+(s); k, \beta)$ is the electric field Green tensor connecting two points just outside the perimeter of the j 'th hole. The mode has been normalised according to

$$\frac{1}{2} \int_{A_{\infty}} d^2 \mathbf{r} [\hat{\mathbf{e}}_1(\mathbf{r}) \times \hat{\mathbf{h}}_1^*(\mathbf{r})] \cdot \hat{\mathbf{z}} = 1, \quad (6)$$

where the integral is over the entire cross-section of the fibre (the x - y plane) and $\hat{\mathbf{z}}$ is a unit vector along the axial direction. Note that with this choice of mode normalisation, the mode group velocity does not explicitly appear in the expression for loss, in contrast to the formulation in [16], which normalises the mode according to energy rather than power.

The dependence on the surface roughness within Eq. (5) is contained solely within the function $\tilde{\Psi}_j(s, s'; \Delta\beta)$, which is given by the discrete Fourier transform of the roughness power spectrum around the hole perimeter. For SCW roughness, the spectrum given in Eq. (3) leads to the form

$$\tilde{\Psi}_j(s, s'; \Delta\beta) = \frac{k_B T_g}{\sigma} \frac{1}{S_j} \sum_{m=-\infty}^{\infty} \frac{\exp[ik_s^{(m)}(s-s')]}{[k_s^{(m)2} + \Delta\beta^2]} \quad (7)$$

for the j 'th hole with perimeter length S_j . This function can be expressed in terms of hypergeometric functions in the general case, but for $\Delta\beta S_j \gg 1$ it simplifies to the extended 2-D surface form

$$\tilde{\Psi}(s, s'; \Delta\beta) = \frac{k_B T_g}{\sigma} \frac{1}{2|\Delta\beta|} \exp(-|\Delta\beta(s-s')|). \quad (8)$$

Equation (5) not only determines the total loss due to the interface roughness scattering, it can also be used to find the angular distribution of the scattered power as a function of the angle θ to the fiber axis. If the fiber is surrounded by a medium of index n_m , β is directly related to the angle θ as measured in this medium by [8]

$$\beta = n_m k \cos \theta, \quad (9)$$

so that a change of variable from β to θ in Eq. (5) makes the desired connection.

The non-separable form of the function $\tilde{\Psi}(s, s'; \Delta\beta)$ with respect to variations along the axial direction and around the hole perimeter is evident in Eq. (8). At large $\Delta\beta$, corresponding to short axial length scales, the exponential term ensures that only points spaced closer than of order $1/\Delta\beta$ in the perimeter coordinate remain correlated. Even for $\Delta\beta \sim 2k$, the electromagnetic terms within the integrand of Eq. (5) vary too rapidly for the equation to be simplified to a single integration around each hole perimeter involving the imaginary part of

the Green tensor evaluated at a single spatial point (which is directly related to the local density of states). As $\Delta\beta$ becomes smaller, the correlations around the perimeter become more and more long ranged, so that the scattered power dependence on β (or equivalently on angle θ) is strongly influenced by the off-diagonal (in spatial coordinate) variations of the Green tensor, as well as on the mode field variations around the hole perimeters.

The electromagnetic terms within Eq. (5) can be calculated using suitable numerical algorithms. The Green tensor can be calculated using, for example, the finite difference time domain method [16], the boundary element approach [17] or, for circular holes, the multipole method [18-21]. In section 4 the multipole method is used to calculate both the Green tensor and the mode field distribution for solid core PCF.

4. Roughness scattering loss in solid core photonic crystal fiber

The roughness scattering dependence on β can be inferred from angular resolved measurements of the light scattered from the guiding mode of the fiber [8]. The experimental technique involves immersing a section of the fiber which has been stripped of its outer protective coating in index matching fluid contained within a cylindrical vessel. Light emerging from the vessel is focused onto a photodetector array. By repeated rotation of the sample, the light escaping from the stripped region of fiber can be measured as a function of direction over all angles θ to the fiber axis. Stray light from the rest of the fiber (*i.e.* other than from the stripped section) is shielded by black tubing. The geometrical deformations in the outer holes of the cladding vary slowly (compared to the wavelength λ) along the fiber axis direction so they do not lead to a substantial modification in the β -dependence of the escaping light.

Figure 1(a) shows the measured scattered power $P(n)$ for the fiber shown as an inset to the figure, plotted as a function of effective index $n=\beta/k$. Obliquity factors are included so that $P(n)dn$ is a measure of the power lost to modes with effective indices between n and $n+dn$. A secondary axis showing the angle θ to the fiber axis, as measured in index matching fluid of refractive index $n_m=1.446$, is also provided. To obtain the measurement, laser light of 1550 nm wavelength was coupled into one end of the fiber and the stripped section, which was of length 5.5mm, was placed many meters from the input end to minimize power in modes other than the fundamental. The fiber was twisted about its axis within the cylindrical vessel so that an average over azimuthal angles was achieved. The trace of $P(n)$ shows a general decrease in power as the difference in effective index to the fundamental mode (which has an index of $n_1\sim 1.40$) increases, which confirms that length-scales longer than the wavelength are responsible for most of the loss so that the scattering is non-Rayleigh in nature.

The fiber studied in the experiment has a pitch (distance between nearest neighbor hole centers) of around 2.85 μm and a core diameter of about 2.8 μm . The holes at such a high air filling fraction are deformed somewhat from circular. The fiber was modeled by keeping the same pitch but approximating the holes to being circular of diameter 2.74 μm . Equation (5) was used with the capillary wave roughness spectrum of Eq. (3) and the electromagnetic terms calculated using the multipole method. The result at a wavelength of 1.55 μm is shown in Fig. 1(b) for comparison with the experimental result. Clear similarities exist between the two traces despite the geometrical approximations incorporated in the calculation. The bumps and dips in the n dependence are identified with an effective index dependence of the density of states. There is, however, a notable asymmetry in the shape of these features between positive and negative index n . This is because the range of the correlations around each hole perimeter decreases with increasing index difference to the forward propagating (*i.e.* positive index) fundamental mode, as discussed in the previous section.

The plot in Fig. 1(b) shows a narrow region of low scattered intensity near the air light line ($n=1$) which is associated with the existence of a cladding band gap over this restricted effective index range. The plot in Fig. 1(a) for the experimental fiber shows no such feature as the deformation of the holes has closed the gap, as was verified by numerical simulation of the experimental geometry using a plane-wave code. The cladding cut-off, which is identified as

the effective index beyond which the scattered intensity becomes strongly suppressed, is approximately 1.06 from the experimental measurement but around 1.1 for the theoretical plot, the difference being mainly due to the higher air filling fraction in the cladding of the fabricated fiber compared to the fraction in the modeled fiber.

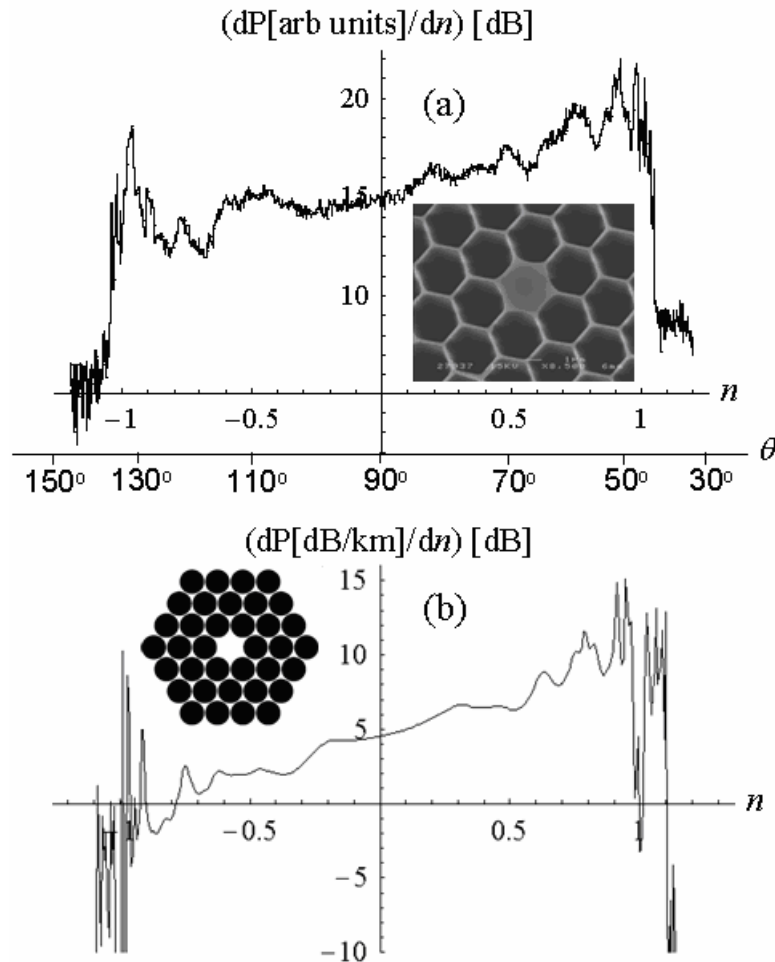


Fig. 1. (a) The measured scattered power as a function of effective index n for a PCF with pitch approximately $2.85 \mu\text{m}$ and core diameter about $2.8 \mu\text{m}$ at a wavelength of $1.55 \mu\text{m}$. A SEM of the structure are included as an inset. In (b), the calculated scattered power due to SCW roughness is shown for a PCF with pitch $2.85 \mu\text{m}$ composed of circular holes of diameter $2.74 \mu\text{m}$. The wavelength is again $1.55 \mu\text{m}$.

The overall decaying trend in the scattered intensity as n becomes more detuned from the index n_1 of the fundamental mode shows some difference between experiment (Fig. 1(a)) and theory (Fig. 1(b)). The experimental plot shows a slightly weaker dependence on $n_1 - n$ than the theoretical one. This can only in part be explained as due to reflections occurring at the end-face of the experimental fiber causing excitation of the backward propagating guided mode and to a Rayleigh component from bulk-material scattering. Since the axial fluctuations of the model spectrum seem to fit well with AFM measurements (albeit with some experimental uncertainty), the slight discrepancy may be due to inter-interface interactions causing a modification in the nature of the correlations around the perimeter of each hole.

The scattered power as a function of both angle θ to the fiber axis and azimuthal angle ϕ is a far more sensitive probe of the fiber microstructure than the azimuthally integrated form shown in Fig. 1. The dependence can be calculated using Eq. (30) of appendix A, which involves the far-field Green tensor together with the roughness spectrum and the mode field distribution. The far-field form of the Green tensor is readily calculated using the multipole approach [20]. Figure 2 shows the calculated dependence for a PCF with pitch $2.0\ \mu\text{m}$ and hole diameter $1.96\ \mu\text{m}$. The radial coordinate in the plot is defined by $n_g - n$, and the azimuthal coordinate is ϕ . An average over the two polarization states associated with the fundamental spatial mode has been taken.

The distribution of the scattered light in Fig. 2 reflects the angular dependence of the mode density. Measurements of the pattern scattered from guided light provide a non-destructive test of the local microstructure around a guiding core which is more easily interpreted than measurement of the scattering of externally incident light which impinges directly upon the side of a stripped section of fiber [22]. The pattern exemplified by the plot in Fig. 2 resembles that obtained from fluorescence measurements on a (suitably scaled) similar fiber with the core doped with an active species such as Er^{3+} [20]. Instead of the point dipole sources associated with fluorescing Er^{3+} ions, the roughness acts as a correlated source for scattered light at the hole interfaces.

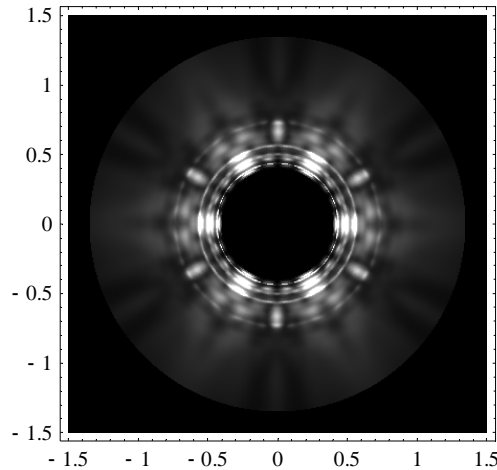


Fig 2. Calculated angular distribution of power scattered due to surface roughness from a solid core PCF with pitch $\Lambda=2.0\ \mu\text{m}$ and hole diameter $1.96\ \mu\text{m}$. The wavelength is $1.55\ \mu\text{m}$.

5. Wavelength scaling of loss

The total loss due to the roughness scattering can be calculated using Eq. (5). The integrand shows rapid variations along the real β -axis, so the computation is performed by deforming the contour of integration into the complex plane. More details of the calculation are given in appendix B.

Figure 3 shows the calculated SCW roughness scattering loss plotted against wavelength λ for a solid core PCF with pitch $1.5\ \mu\text{m}$ and circular holes of diameter $1.44\ \mu\text{m}$. The roughness loss is seen to be only weakly dependent on the wavelength. A trace showing approximately 50 times the contribution to the loss from bulk Rayleigh scattering, which has a $1/\lambda^4$ dependence, is included for comparison. A fit of the form $1/\lambda^\nu$ to the roughness loss yields an index $\nu=0.70$ as a best fit. The roughness loss for such a small core fiber is far greater than the loss arising from bulk Rayleigh scattering and is confirmed as being the dominant source of loss away from water absorption peaks and the IR absorption edge. The

wavelength dependence of the roughness loss is weakened compared to the $1/\lambda^4$ bulk-Rayleigh form both because the normalized guided mode field intensity at the interfaces varies approximately as λ^2 [7], and because the roughness power spectrum increases with length scale.

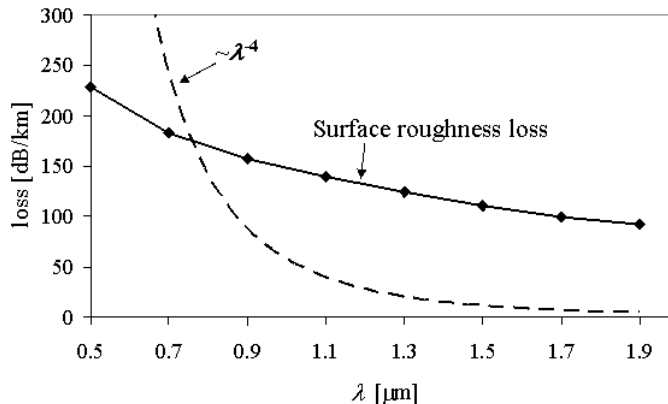


Fig. 3. The wavelength dependence of roughness loss calculated for a solid core PCF with pitch $1.5\mu\text{m}$ and circular holes of diameter $1.44\mu\text{m}$. A curve with $1/\lambda^4$ dependence, approximately 50 times the strength of the bulk Rayleigh scattering contribution, is included for comparison.

Figure 4 shows the measured loss of a fabricated fiber with a similar core size to the modeled example. A SEM of the structure is provided as an inset. The peaks around $0.95\mu\text{m}$, $1.25\mu\text{m}$ and $1.39\mu\text{m}$ are due to OH⁻ absorption, but the remaining dependence is assumed to be almost entirely due to surface roughness scattering. The dashed line in the plot has a $1/\lambda^{1.24}$ dependence which indicates that the roughness loss of the fabricated fiber varies slightly more rapidly with wavelength than predicted for the model fiber and the assumed roughness spectrum. This is in keeping with the slightly flatter dependence of the measured scattered intensity with angle compared with the modeled result, a feature which was noted in section 4. The loss of the fabricated fiber is between 1.1 and 2.0 times higher than that calculated for the model fiber over the wavelength range $0.6\text{-}1.7\mu\text{m}$. The similarity in the measured and calculated values shows that SCW roughness provides a credible explanation for the majority of the observed loss in small solid-core PCF. In part the persistent underestimate of the loss from the modeling is due to the deformation in the holes which surround the core in the fabricated fiber causing an increase in the field intensity at the interfaces.

As the core size of the PCF increases or the hole size decreases, the separation in β of the fundamental mode from the cladding cut-off (or other core guided modes if any exist) becomes ever smaller. The large scale (i.e. small k_{SCW}) divergence associated with the assumed form of the SCW roughness spectrum eventually leads to an overestimate of the loss. A loss of 0.27 dB/km has been ascribed to surface roughness scattering at a wavelength of $1.55\mu\text{m}$ for a fiber with pitch $4.2\mu\text{m}$ incorporating holes with diameter $1.85\mu\text{m}$ [7]. For such a fiber, the β -detuning of the fundamental mode from the cladding cut-off is just $0.031\mu\text{m}^{-1}$, and evaluation of Eq. (5) using the model SCW spectrum leads to a calculated loss of around 6 dB/km . Clearly it is necessary to introduce a long length scale cut-off to the roughness spectrum. The physical mechanism giving rise to the cut-off is not currently understood, but it is plausible that the interaction between SCWs on adjacent holes plays a key role.

A long-scale cut-off of size L_{cut} can be phenomenologically introduced to the roughness spectrum by considering the modified form

$$\tilde{\Psi}'_m(\beta) = \frac{k_B T_g}{\sigma} \frac{1}{S} \frac{1}{[k_s^{(m)2} + \beta^2 + k_{cut}^2]}, \quad (10)$$

where $k_{cut} = 2\pi/L_{cut}$. Roughness scattering calculations using this spectral form show that in order to obtain a loss comparable to the experimental value for the PCF with pitch $\Lambda=4.2 \mu\text{m}$, it is necessary that L_{cut} is taken to have a value around $20 \mu\text{m}$.

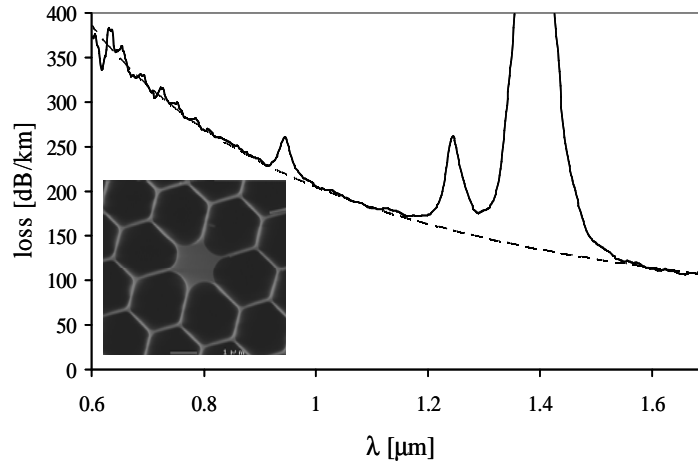


Fig. 4. The measured loss vs. wavelength for a fabricated PCF with a core diameter of around $1.5 \mu\text{m}$. A SEM of the structure is included as an inset. The dashed curve has a dependence of $\lambda^{-1.24}$.

6. Conclusions

The guided mode propagation loss in solid core photonic crystal fibers (PCFs) due to hole interface roughness scattering has been calculated assuming the roughness is due to frozen-in surface capillary waves (SCWs). For small-core fibers, the loss computed using a simple continuum theory for the SCW spectrum is found to give values within a factor of 2 of measured loss values of fabricated fibers. For such fibers, the interface roughness scattering is confirmed as being the dominant loss mechanism over a broad range of wavelengths and is characterized by a weak dependence of the loss on wavelength. For fibers with a larger core size, it is found that a long length scale cut-off must be introduced to the roughness spectrum in order to gain correspondence with measured loss values.

Comparison of the computed scattering dependence on angle with experimental measurements suggests that the roughness spectrum is slightly flatter than the model SCW spectrum. A similar conclusion is inferred by comparison of the computed and measured dependence of the loss on wavelength. A more sophisticated theory of frozen-in SCWs on the interfaces of closely spaced holes within PCF is clearly necessary to resolve the small discrepancies and to provide an explanation for the inferred long length scale cut-off in the spectrum. A detailed understanding of such a theory may lead the way to further loss reduction in both band-gap and solid core photonic crystal fibers.

Appendix A: Scattering from interface roughness

The roughness amplitude at the glass / air interfaces of PCFs is far smaller than the wavelength of the guided light. Thus the scattering due to the roughness can be calculated using perturbation theory. Since the index step at the interfaces is not small, it is most expedient to calculate the scattering using the framework of local mode coupling theory, even

though the unperturbed modes can be considered as invariant along the fiber. It will be assumed that the roughness amplitude is small compared to a small scale cut-off length in the roughness spectrum, so a complicated local-field calculation can be avoided [12,15].

From [12], the amplitude b_p of a mode labeled by the index p evolves along the fiber (the direction $0z$) according to

$$\frac{db_p}{dz} - i\beta_p b_p = \sum_q \zeta_p C_{pq} b_q, \quad (11)$$

where β_p is the propagation constant of the p 'th mode (the wavevector component along the fiber direction). The factor ζ_p takes the value +1 if p corresponds to a forward propagating mode or -1 if p corresponds to a backward propagating mode. The summation is over all transverse modes of the fiber, labeled here by an index q . The index q is understood to be a discrete label for guided modes of the system and to be continuous for radiation modes. The summation over the latter type of mode is to be interpreted an integration over the continuous index. The coupling coefficients $\{C_{pq}\}$, written in a form appropriate for arbitrary index step, are given by

$$C_{pq}(z) = \frac{k}{4} \left(\frac{\epsilon_0}{\mu_0} \right)^{1/2} \frac{1}{\Delta\beta_{pq}} \int_{\mathbf{x}\text{-section}} d^2 \mathbf{r} \left\{ \begin{aligned} & \left[\hat{\mathbf{e}}_p^* \cdot \hat{\mathbf{e}}_q - (\hat{\mathbf{e}}_p^* \cdot \hat{\mathbf{n}})(\hat{\mathbf{e}}_q \cdot \hat{\mathbf{n}}) \right] \frac{\partial n^2}{\partial z} - \\ & \left(n^2 \hat{\mathbf{e}}_p^* \cdot \hat{\mathbf{n}} \right) \left(n^2 \hat{\mathbf{e}}_q \cdot \hat{\mathbf{n}} \right) \frac{\partial}{\partial z} \left(\frac{1}{n^2} \right) \end{aligned} \right\}, \quad (12)$$

where k is the wavenumber of the radiation ($k = 2\pi/\lambda$), $\Delta\beta_{pq} = \beta_p - \beta_q$ is the difference in propagation constant between the p 'th and the q 'th modes, and n is the refractive index distribution of the perturbed fiber. The electric fields of the p 'th and q 'th normalized transverse modes are denoted $\hat{\mathbf{e}}_p$ and $\hat{\mathbf{e}}_q$ respectively, and $\hat{\mathbf{n}}$ is a spatially dependent unit vector chosen to be normal to the dielectric interfaces. The modes are normalized according to the convention in [12].

It will be assumed that light in a forward propagating guided mode, labeled by an index $p=1$, is incident at $z=0$. As the scattering is weak, Eq. (11) can be integrated to yield for the amplitude in mode 1 a distance L along the fiber:

$$b_1(L) = b_1(0) \exp(i\beta_1 L) \left\{ 1 + \sum_q \int_0^L dz' \int_{z'-L}^{z'} dz_d \eta_q(z_d) C_{1q}(z') C_{q1}(z'-z_d) \exp[i(\beta_q - \beta_1)z_d] \right\}. \quad (13)$$

The function $\eta_q(z_d)$ takes the value 1 either if $z_d > 0$ and q labels a forward propagating mode or if $z_d < 0$ and q labels a backward propagating mode, otherwise it is zero.

The rate of loss, γ_1 , from mode 1, is determined from

$$\gamma_1 = \frac{1}{L} \left(1 - \frac{\langle |b_1^2(L)|^2 \rangle}{|b_1(0)|^2} \right) = -\frac{2}{L} \text{Re} \left[\sum_q \int_0^L dz' \int_{-\infty}^{z'} dz_d \eta_q(z_d) \langle C_{1q}(z') C_{q1}(z'-z_d) \rangle \exp[i(\beta_q - \beta_1)z_d] \right], \quad (14)$$

where the angled brackets denote an ensemble average over a statistical ensemble which describes the roughness fluctuations.

The length L is assumed long compared to the wavelength and any relevant correlation length scale of the surface roughness, but small enough that the scattering from the

fundamental mode is weak (*i.e.* $L \ll 1/\gamma_1$). Assuming the nature of the surface roughness does not change along the fiber (statistical homogeneity), the rate of loss can then be determined from

$$\gamma_1 = -2 \operatorname{Re} \left[\sum_q \int_{-\infty}^{\infty} dz_d n_q(z_d) \langle C_{1q}(0) C_{q1}(z_d) \rangle \exp[i(\beta_q - \beta_1)z_d] \right]. \quad (15)$$

It will be assumed that the physical process which forms the roughness does not lead to a change in refractive index within the medium, *i.e.* its sole effect is to cause a small geometric perturbation to the dielectric interfaces. The refractive index distribution of the perturbed fiber may be then written as $n^2(\mathbf{r}, z) = n_0^2(\mathbf{r} + \mathbf{u}(\mathbf{r}, z))$, where $n_0^2(\mathbf{r})$ is the refractive index distribution of the unperturbed (z -independent) fiber and $\mathbf{u}(\mathbf{r}, z)$ defines the perturbations to the interfaces. \mathbf{r} is a 2D position vector in the plane transverse to the fiber axis. The refractive index will be assumed to undergo a discontinuous step from a value n_g within the glass to unity within a hole as an interface is traversed. Since the displacements $\mathbf{u}(\mathbf{r}, z)$ are small in amplitude, the required derivatives of the dielectric distribution can then be determined from

$$\begin{aligned} \frac{\partial n^p(\mathbf{r}, z)}{\partial z} &= \nabla_{\parallel} n_0^p(\mathbf{r}') \Big|_{\mathbf{r}'=\mathbf{r}+\mathbf{u}(\mathbf{r}, z)} \cdot \frac{\partial \mathbf{u}(\mathbf{r}, z)}{\partial z} \\ &\equiv (n_g^p - 1) \sum_{j=1}^{N_{\text{holes}}} \oint_{\text{interface}}^{j^{\text{th}} \text{ hole}} ds \delta(\mathbf{r} - \mathbf{r}_j(s)) \frac{\partial h_j(s, z)}{\partial z} \end{aligned} \quad (p = 2, -2), \quad (16)$$

where $h_j(s, z) = \hat{\mathbf{n}}_j(s) \cdot \mathbf{u}(\mathbf{r}_j(s), z)$ is the roughness height function for the j 'th hole, with s a spatial coordinate (with distance measure) which defines a position on the unperturbed interface via the function $\mathbf{r}_j(s)$. The integrals over s extend around each of the N_{holes} hole perimeters and the delta function ensures that the dielectric derivatives are only non-vanishing at the hole interfaces. The unit vector $\hat{\mathbf{n}}_j(s)$ is the outward normal to the j 'th hole interface.

The required coupling coefficients, using Eqs. (12) and (16), are then given by

$$C_{pq}(z) = \frac{k}{4} \left(\frac{\epsilon_0}{\mu_0} \right)^{1/2} \frac{1}{\Delta \beta_{pq}} \sum_{j=1}^{N_{\text{holes}}} \oint_{\text{interface}}^{j^{\text{th}} \text{ hole}} ds \left\{ \frac{(n_g^2 - 1) \hat{\mathbf{e}}_p^* \cdot \hat{\mathbf{e}}_q - (\hat{\mathbf{e}}_p^* \cdot \hat{\mathbf{n}}_j(s)) (\hat{\mathbf{e}}_q \cdot \hat{\mathbf{n}}_j(s))}{(n_g^{-2} - 1) (n_0^2 \hat{\mathbf{e}}_p^* \cdot \hat{\mathbf{n}}_j(s)) (n_0^2 \hat{\mathbf{e}}_q \cdot \hat{\mathbf{n}}_j(s))} \right\} \frac{\partial h_j(s, z)}{\partial z}. \quad (17)$$

The quantity within curly brackets can be rewritten as

$$\left\{ \frac{(n_g^2 - 1) \hat{\mathbf{e}}_p^* \cdot \hat{\mathbf{e}}_q - (\hat{\mathbf{e}}_p^* \cdot \hat{\mathbf{n}}_j(s)) (\hat{\mathbf{e}}_q \cdot \hat{\mathbf{n}}_j(s))}{(n_g^{-2} - 1) (n_0^2 \hat{\mathbf{e}}_p^* \cdot \hat{\mathbf{n}}_j(s)) (n_0^2 \hat{\mathbf{e}}_q \cdot \hat{\mathbf{n}}_j(s))} \right\} = (n_g^2 - 1) I_j^{(pq)}(s), \quad (18)$$

with

$$I_j^{(pq)}(s) = \left\{ \hat{\mathbf{e}}_p^*(\mathbf{r}_j^+(s)) \cdot \hat{\mathbf{e}}_q(\mathbf{r}_j^+(s)) + \left[\hat{\mathbf{e}}_p^*(\mathbf{r}_j^-(s)) \cdot \hat{\mathbf{n}}_j(s) - \hat{\mathbf{e}}_p^*(\mathbf{r}_j^+(s)) \cdot \hat{\mathbf{n}}_j(s) \right] \left[\hat{\mathbf{e}}_q(\mathbf{r}_j^+(s)) \cdot \hat{\mathbf{n}}_j(s) \right] \right\}. \quad (19)$$

In Eq. (19), $\mathbf{r}_j^{(+)}(s)$ refers to a point just outside the interface of the j 'th hole (*i.e.* within the glass), and $\mathbf{r}_j^{-}(s)$ is a position just inside the interface. $I_j^{(pq)}(s)$ remains invariant if all the + superscripts are replaced with – superscripts, and all the – superscripts are simultaneously exchanged for + superscripts.

Inserting Eq. (17) into Eq. (15) and making use of Eq. (18), the loss can be expressed as

$$\gamma_1 = \frac{k^2}{8} \left(\frac{\epsilon_0}{\mu_0} \right) (n_g^2 - 1)^2 \sum_q \frac{1}{\Delta\beta_{1q}^2} \operatorname{Re} \left[\sum_{j=1}^{N_{\text{holes}}} \oint_{\text{perimeter}}^{N_{\text{holes}}} d s \mathbf{I}_j^{(1q)}(s) \oint_{\text{perimeter}}^{N_{\text{holes}}} d s' \mathbf{I}_k^{(q1)}(s') \times \int_{-\infty}^{\infty} d z_d \eta_q(z_d) \exp(i\Delta\beta_{q1} z_d) \frac{\partial^2}{\partial^2 z_d} \Psi_{jk}(s, s'; z_d) \right], \quad (20)$$

where

$$\Psi_{jk}(s, s'; z_d) = \langle h_j(s, 0) h_k(s', z_d) \rangle \quad (21)$$

and the assumed statistical stationarity has ensured that

$$\left\langle \frac{\partial h_j(s, z)}{\partial z} \Big|_{z=0} \frac{\partial h_k(s', z)}{\partial z} \Big|_{z=z_d} \right\rangle = - \frac{\partial^2}{\partial^2 z_d} \Psi_{jk}(s, s'; z_d). \quad (22)$$

Assuming that the roughness on each hole is statistically independent so that

$$\Psi_{jk}(s, s'; z_d) = \Psi_j(s, s'; z_d) \delta_{jk}, \quad (23)$$

and integrating over z_d by parts twice, the loss is given by

$$\gamma_1 = \frac{k^2}{8} \left(\frac{\epsilon_0}{\mu_0} \right) (n_g^2 - 1)^2 \operatorname{Re} \left[\sum_{j=1}^{N_{\text{holes}}} \oint_{\text{perimeter}}^{N_{\text{holes}}} d s \oint_{\text{perimeter}}^{N_{\text{holes}}} d s' \int_{-\infty}^{\infty} d z_d \sum_q \mathbf{I}_j^{(1q)}(s) \mathbf{I}_j^{(q1)}(s') \exp(i\Delta\beta_{q1} z_d) \eta_q(z_d) \Psi_j(s, s'; z_d) \right]. \quad (24)$$

The loss can be expressed in terms of the electric field Green tensor describing propagation within the unperturbed waveguide by using the relation

$$\sum_q \eta_q(z_d) \hat{\mathbf{e}}_q(\mathbf{r}) \hat{\mathbf{e}}_q^H(\mathbf{r}') \exp(i\beta_q z_d) = 4ik \left(\frac{\mu_0}{\epsilon_0} \right)^{1/2} \mathbf{G}_{3D}(\mathbf{r} + z_d \hat{\mathbf{z}}, \mathbf{r}' + 0\hat{\mathbf{z}}; k) \quad (25)$$

to make the connection

$$\sum_q \mathbf{I}_j^{(1q)}(s) \mathbf{I}_j^{(q1)}(s') \eta_q(z_d) \exp(i\beta_q z_d) = 4ik \left(\frac{\mu_0}{\epsilon_0} \right)^{1/2} \times \hat{\mathbf{e}}_1^H(\mathbf{r}_j^-(s')) \mathbf{G}_{3D}(\mathbf{r}_j^+(s') + z_d \hat{\mathbf{z}}, \mathbf{r}_j^+(s) + 0\hat{\mathbf{z}}; k) \hat{\mathbf{e}}_1(\mathbf{r}_j^-(s)) \quad (26)$$

Use of Eq. (26) in Eq. (24) leads to

$$\gamma_1 = - \frac{k^3}{4\pi} \left(\frac{\epsilon_0}{\mu_0} \right)^{1/2} (n_g^2 - 1)^2 \operatorname{Im} \left[\sum_{j=1}^{N_{\text{holes}}} \oint_{\text{perimeter}}^{N_{\text{holes}}} d s \oint_{\text{perimeter}}^{N_{\text{holes}}} d s' \int d\beta \hat{\mathbf{e}}_1^H(\mathbf{r}_j^-(s')) \mathbf{G}_{2D}(\mathbf{r}_j^+(s'), \mathbf{r}_j^+(s); k, \beta) \hat{\mathbf{e}}_1(\mathbf{r}_j^-(s)) \tilde{\Psi}_j(s, s'; \beta_1 - \beta) \right], \quad (27)$$

where

$$\mathbf{G}_{2D}(\mathbf{r}, \mathbf{r}'; k, \beta) = \int_{-\infty}^{\infty} d z_d \exp(-i\beta z_d) \mathbf{G}_{3D}(\mathbf{r} + z_d \hat{\mathbf{z}}, \mathbf{r}' + 0\hat{\mathbf{z}}; k) \quad (28)$$

and

$$\tilde{\Psi}_j(s, s'; \Delta\beta) = \int_{-\infty}^{\infty} dz_d \exp(-i\Delta\beta z_d) \Psi_j(s, s'; z_d). \quad (29)$$

Equation (27) expresses the loss in terms of the spectrum of the surface fluctuations, the field distribution of the guiding mode, the dielectric permittivity step between glass and air and the electric field Green tensor which describes propagation of radiation around the hole interfaces.

The loss due to scattering into β -values between β and $\beta + \delta\beta$ can be directly extracted from Eq. (27) and related to the loss into a range of angles θ to $\theta + \delta\theta$ to the fiber axis as described in section 3. To obtain the scattered power dependence on both θ and the azimuthal angle ϕ , a Born series expansion can be invoked [12]. The ambiguity arising due to the discontinuity in normal \mathbf{E} -field can be removed by ensuring that integration over ϕ leads to a form which is consistent with Eq. (27). The calculation leads to the loss $\gamma_1(\theta, \phi) \delta\Omega$ into a solid angle element $\delta\Omega = \sin\theta \delta\theta \delta\phi$ being given in the far-field by

$$\gamma_1(\theta, \phi) = \frac{1}{4\pi} \left(\frac{\epsilon_0}{\mu_0} \right)^{1/2} k^5 n_g (n_g^2 - 1)^2 \sin\theta \operatorname{Re} \operatorname{Lim}_{R \rightarrow \infty} R \operatorname{Re} \sum_j \oint_{\text{perimeter}}^{j^{\text{th}} \text{ hole}} ds \oint_{\text{perimeter}}^{j^{\text{th}} \text{ hole}} ds' \tilde{\Psi}(s, s'; \beta_1 - \beta) \times \hat{\mathbf{e}}_1^H(\mathbf{r}_j^-(s)) \mathbf{G}_{2D}^H(R\hat{\mathbf{o}}, \mathbf{r}_j^+(s); k, \beta) \mathbf{G}_{2D}(R\hat{\mathbf{o}}, \mathbf{r}_j^+(s); k, \beta) \hat{\mathbf{e}}_1(\mathbf{r}_j^-(s)) \quad (30)$$

where $\hat{\mathbf{o}} = (\cos\phi, \sin\phi)$ and it has been assumed that the fiber is surrounded by index matching fluid with an index equal to that of the glass, so that $\beta = n_g k \cos\theta$ and all scattering is due to the holes in the fiber microstructure.

Appendix B: Calculation of the total loss due to roughness scattering

Sharp variations with β occur within the integrand of Eq. (5) due to the occurrence of leaky modes or resonances. Higher order guided modes as well as the fundamental may exist beyond the cladding cut-off, which for an infinite cladding give rise to simple poles of the Green tensor at their propagation constant eigenvalues. For a finite cladding the modes suffer some degree of confinement loss so that the poles are shifted slightly from the real axis. The rapid variations associated with the occurrence of poles close to the integration path in Eq. (5) means that direct integration along the real β -axis is impractical, so the integration contour is deformed into the complex plane.

The analytic properties of the Green tensor in the complex plane have been explored in [19]. The simple poles associated with the leaky modes are constrained to the quadrants $\operatorname{Re}[\beta] > 0, \operatorname{Im}[\beta] > 0$ and $\operatorname{Re}[\beta] < 0, \operatorname{Im}[\beta] < 0$ in order to satisfy causality. Branch cuts extend outward along the real-axis from the points $\pm\beta_g$, where $\beta_g = n_g k$. The roughness function $\tilde{\Psi}_j(s, s'; \beta_1 - \beta)$ for capillary waves associated with the j^{th} hole introduces further poles to the integrand at β -values given by

$$\beta = \beta_1 + i2\pi m/S_j, \quad (31)$$

where m is an integer. To exclude the contribution of scattering from mode 1 into itself and into its polarization partner (labeled mode 2), which in fact diverges for the modal capillary spectrum due to the presence of a double-pole in the roughness function $\tilde{\Psi}_j(s, s'; \Delta\beta)$ at $\Delta\beta=0$, the contribution of these modes is subtracted from the Green tensor so that

$$\mathbf{G}_{2D}(\mathbf{r}, \mathbf{r}'; k, \beta) \rightarrow \mathbf{G}_{2D}(\mathbf{r}, \mathbf{r}'; k, \beta) - \left(\frac{\epsilon_0}{\mu_0} \right)^{1/2} \frac{1}{4k} \sum_{q=1}^2 \frac{\hat{\mathbf{e}}_q(\mathbf{r}) \hat{\mathbf{e}}_q^H(\mathbf{r}')}{\beta_q - \beta}. \quad (32)$$

The deformed path used in the calculation has an end-point given by $\beta_U = \beta_1 - \delta\beta$, where $\delta\beta$ is a small positive real value chosen such that β_U is larger than the propagation constant at the cladding cut-off and, if any exist, of any guided mode other than modes 1 and 2. The start point is chosen to lie between $-\beta_g$ and $-\beta_1$, so that scattering into backward traveling fundamental modes is included. The structure of the integrand of (5) in the complex plane and the chosen deformed path is shown schematically in Fig. 5.

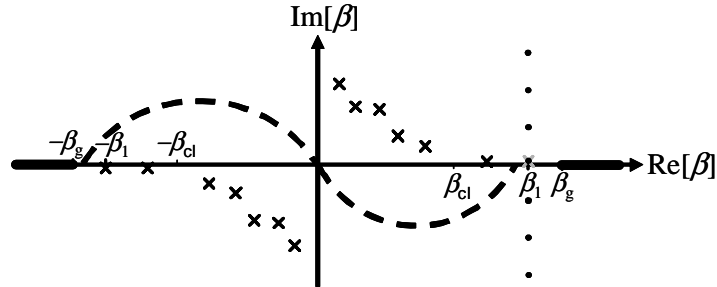


Fig. 5. A plot of the complex plane schematically showing the analytic structure of the integrand in Eq. (5). The poles associated with the Green tensor are shown by crosses and those of the roughness function $\tilde{\Psi}(s, s'; \beta - \beta_1)$ by dots. The Green tensor poles due to forward propagating modes 1 and 2 are shown in grey and have been subtracted. The thick continuous lines indicate branch cuts. β_g is the β -value of the cladding cut-off and $\beta_g = n_g k$. The path of integration is deformed from the real β -axis to the dashed curve shown.